Accelerometer Placement in Active Flutter Suppression Systems

Bradley S. Liebst*
University of Minnesota, Minneapolis, Minnesota

An elementary study of the placement of accelerometers when used as sensors in active flutter suppression systems is presented. The model analyzed is a two-dimensional typical section with various combinations of leading- and trailing-edge controllers. The relationship between the control surface placement and accelerometer placement is examined. The results for the numerical examples presented show that accelerometers must be on the same side of the center of gravity as the control surface or right half-plane transmission zeros will arise. The detrimental effects of the right half-plane zeros are discussed in the context of linear-quadratic-regulator plus loop-transfer-recovered observer designs.

Nomenclature

a = distance elastic axis is aft of the midchord, nondimensionalized by b
A = state matrix, see Eq. (5)
b = semichord of section, $c/2$
B = control influence matrix, see Eq. (5)
c = chord of section
C = measurement matrix, see Eq. (6)
c_L = distance leading-edge controller hingeline is aft of the midchord, nondimensionalized by b
c_T = distance trailing-edge controller hingeline is aft of the midchord, nondimensionalized by b
h = downward displacement of elastic axis
$\bar{h}$ = downward displacement of accelerometer position
I = identity matrix
I_α = moment of inertia per unit length of section about the elastic axis
j = $\sqrt{-1}$
K = regulator gain matrix
K_h = stiffness of section in deflection
K_α = torsional stiffness of section about elastic axis
ℓ = distance accelerometer is aft of elastic axis, nondimensionalized by b
L = observer gain matrix
L = lift per unit span
L_α = slope $\partial L/\partial\alpha = 2\pi\rho U^2 b$
L_{β_L} = slope $\partial L/\partial\beta_L = 2(T_{10_L} - \pi)\rho U^2 b$
L_{β_T} = slope $\partial L/\partial\beta_T = 2T_{10_T}\rho U^2 b$
m = mass per unit length of section
M = aerodynamic moment per unit span about elastic axis
M_α = slope $\partial M/\partial\alpha = 2\pi\rho b^2 U^2(a + 1/2)$
M_{β_L} = slope $\partial M/\partial\beta_L = \rho b^2 U^2[2aT_{10_L} - T_{4_L} - 2\pi(a + 1/2)]$
M_{β_T} = slope $\partial M/\partial\beta_T = \rho b^2 U^2(2aT_{10_T} - T_{4_T})$
p = system poles
q = loop-transfer-recovery noise weighting parameter
s = Laplace variable
S_α = static moment of the wing per unit length about elastic axis, $= mx_\alpha b$
$T_{4_{T,L}}$ = control surface constant, $= -\cos^{-1} c_{T,L} + c_{T,L}\sqrt{1 - c_{T,L}^2}$
$T_{10_{T,L}}$ = control surface constant, $= \sqrt{1 - c_{T,L}^2} + \cos^{-1} c_{T,L}$
u = control input commands vector, see Eq. (5)
U = airspeed
U_F = flutter speed
w_G = vertical wind gust
x = state vector, see Eq. (5)
x_α = distance center of gravity is aft of elastic axis, nondimensionalized by b
$\hat{x}$ = state estimate
y = accelerometer measurements vector, see Eq. (6)
$\bar{y}$ = measured vertical acceleration at accelerometer position
z = system transmission zeros
α = angle of attack
β_L = deflection of leading-edge control surface
β_T = deflection of trailing-edge control surface
Γ = gust influence vector, see Eq. (5)
ρ = air density
$\underline{\sigma}$ = minimum singular value
$\bar{\sigma}$ = real part of transfer function
τ = break frequency for first-order actuator dynamics
ω = radian frequency

Superscripts
$^{-1}$ = matrix inverse
^{T} = matrix transpose
$\dot{(\ )}$ = time derivative

Subscripts
T = trailing-edge control
L = leading-edge control

Introduction

OVER the last 20 years, much has been written on the design and implementation of active flutter suppression systems.[1-11] Flight tests of flutter suppression systems were flown as early as 1975.[4] Active flutter control for transport aircraft is discussed in Refs. 4 and 5. More recently, a good deal of active flutter control research has been generated by the DAST (Drones for Aerodynamic and Structural Testing) program.[6-11] Most flutter suppression systems rely on movable aerodynamic surfaces (either leading- or trailing-edge) as the control inputs and accelerometer readings at various posi-

Received May 2, 1986; revision received Jan. 14, 1987.

*Assistant Professor, Department of Aerospace Engineering and Mechanics. Senior Member AIAA.

tions on the wing as the measured outputs. The importance of collocating sensors and actuators in control systems has been demonstrated by several authors.[12,13] Sensor/actuator collocation is important in flutter suppression systems as well. In the course of the author's research on the DAST program, several studies were conducted to determine optimum accelerometer placement.[11] These investigations invariably resulted in best performance whenever accelerometers were placed at or near the control surface hingelines. This paper is an attempt to theoretically justify this particular configuration in general.

Dowell and Horikawa[14] and Edwards[15] provide a great deal of insight into the problem of active flutter control with acceleration feedback by working with the two-dimensional (2-D) typical section. The simplicity of the 2-D typical section provides physical insight into the problem that is obscured by the complicated multiple-degree-of-freedom models presented in the analyses previously described. For this reason, the 2-D typical section incorporating static aerodynamic theory and both leading- and trailing-edge control surfaces, will be utilized in the present analysis as well. References 14 and 15 examined control systems utilizing measurements made at the elastic axis only. As this study will show, the elastic axis is in fact typically a poor location at which to place sensors, and proper chordwise accelerometer positioning can result in significant performance improvements.

A commonly utilized design procedure in modern multi-input/multi-output flutter control systems is to couple full state designs developed with linear-quadratic-regulator (LQR) techniques[5,8,9] with robust estimators developed using the Doyle and Stein procedure[8,16] [commonly referred to as loop-transfer-recovery (LTR)]. All compensators in the present study will be developed in this same manner.

Typical Section Model

Structural/Aerodynamics

The simplest structural/aerodynamic model is chosen to help provide physical insight into the flutter suppression system. Therefore, any conclusions reached are only qualitative in nature. The biggest single limitation on the simple model is the static aerodynamic theory, which will not be able to account for compressibility effects and aerodynamic damping.

The typical section that will be analyzed is shown in Fig. 1. The 2-D typical section is described in detail by Theodorsen.[17] The linearized equations of motion with static aerodynamic assumptions and the inclusion of a vertical gust w_G are

$$I_\alpha \ddot{\alpha} + S_\alpha \ddot{h} + (K_\alpha - M_\alpha)\alpha = M_{\beta_T}\beta_T + M_{\beta_L}\beta_L + (M_\alpha/U)w_G \tag{1}$$

$$m\ddot{h} + S_\alpha \ddot{\alpha} + K_h h + L_\alpha \alpha = -L_{\beta_T}\beta_T - L_{\beta_L}\beta_L - (L_\alpha/U)w_G \tag{2}$$

Actuator Dynamics

If one wishes to take into account control surface actuator dynamics, the simplest model would be a first-order lag at frequency τ.

$$\dot{\beta}_{T,L} + \tau\beta_{T,L} = \tau u_{T,L} \tag{3}$$

where u is the commanded control input.

Accelerometer Measurements

Consider the downward displacement $\bar{h}$ of an accelerometer mounted aft of the elastic axis a distance ℓb, then to first order

$$\bar{h} = h + \ell b\alpha$$

and

$$\bar{y} = \text{measured output} = \ddot{\bar{h}} = \ddot{h} + \ell b\ddot{\alpha} \tag{4}$$

If we have two accelerometers,

$$\bar{y}_1 = \ddot{h} + \ell_1 b\ddot{\alpha}$$

$$\bar{y}_2 = \ddot{h} + \ell_2 b\ddot{\alpha}$$

State-Space Model

One could of course recast the preceding into the first-order form

$$\dot{x} = Ax + Bu + \Gamma w_G \tag{5}$$

$$y = Cx \tag{6}$$

Control System Synthesis

The objective of any feedback control system is to provide good disturbance rejection and stability in the face of uncertainties present in the mathematical model of the physical system. In the present analysis, the disturbance is the vertical gust and the outputs are the various states. Flutter suppression systems will be examined that are designed in two steps, the first being to analyze the problem assuming all the states

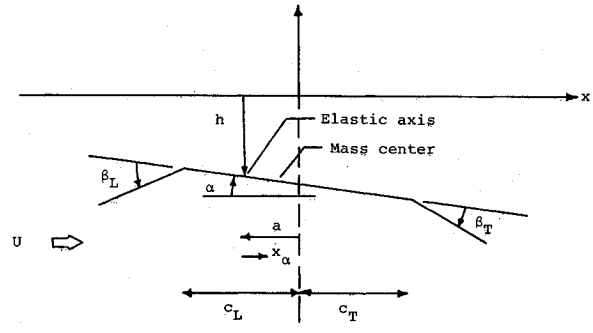

Fig. 1 Diagram of typical section with leading- and trailing-edge control surfaces.

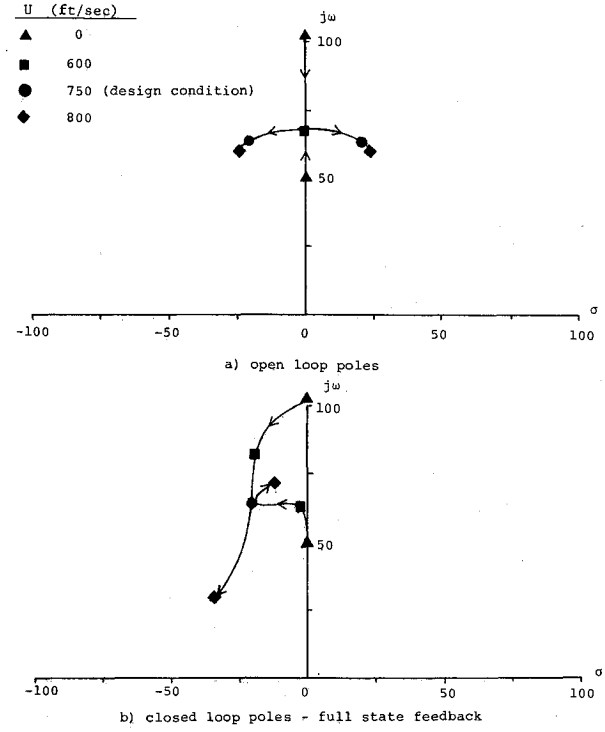

Fig. 2 Root locus of poles for varying velocity for trailing-edge control only.

could be measured, and the second to design an observer that takes the accelerometer measurements and reconstructs an estimate of the state. In the first task, if the state can be measured completely we propose to determine the feedback gain matrix K, where $u = -Kx$, by LQR techniques. The control weighting is chosen to be the identity matrix and the state weighting the zero matrix. This "minimum control energy" weighting is known to move any open-loop poles in the right half-plane to their mirror images in the left half-plane, and leave all other poles unaltered.[18]

For simplicity, we will assume that the vertical gust is a zero mean white noise with unity intensity (the actual intensity is irrelevant since we wish only to show qualitative relationships here). Thus, by solving the appropriate Lyapunov equations, the rms responses for each of the states can be determined from the closed-loop state equation

$$\dot{x} = (A - BK)x + \Gamma w_G$$

The second step in the control system synthesis is to design an observer that utilizes the measurement vector y as its input and outputs a state estimate $\hat{x}$. The Kalman estimator is described as

$$u = -K\hat{x}$$

where

$$\dot{\hat{x}} = A\hat{x} + Bu + L(y - C\hat{x})$$

The closed-loop equation for the full state regulator plus observer system is then

$$\begin{Bmatrix} \dot{x} \\ \dot{\hat{x}} \end{Bmatrix} = \begin{bmatrix} A & -BK \\ LC & A - BK - LC \end{bmatrix} \begin{Bmatrix} x \\ \hat{x} \end{Bmatrix} + \begin{Bmatrix} \Gamma \\ 0 \end{Bmatrix} w_G$$

From the preceding, we can get rms h, α, and β's. The LTR procedure involves picking appropriate fictitious plant noise intensity to achieve stability robustness. Doyle and Stein[16] show that a robust Kalman estimator is obtained by adding a fictitious noise qBB^T directly to the control input of the plant during the estimator design. For $q = 0$, the ordinary Kalman estimator results. As q is increased, the estimator becomes more robust; however, rms response increases. If the sensors result in an output transfer function

$$G_m(s) = C(sI - A)^{-1}B \tag{7}$$

that has no right half-plane transmission zeros (i.e., minimum phase), the stability characteristics are guaranteed to approach the full state feedback results. The theory dictates that as q is increased, the filter poles tend to the zeros of the plant or to infinity. In essence, the plant is being inverted. This explains why nonminimum phase plants (or plants with right half-plane zeros) may have stability robustness problems. The Kalman estimator must be stable; consequently, any poles tending to right half-plane zeros will go to mirror images in the left half-plane instead, and robustness recovery is not guaranteed. We will demonstrate that, in the example flutter suppression system, proper placement of accelerometers will result in minimum phase systems with good robustness and conversely, that improper placement of the accelerometers results in right half-plane zeros and subsequent degradation in system rms performance and stability robustness. For the two control cases, the combined regulator-observer system robustness will be measured in terms of the minimum singular value of the following return difference matrix:

$$I + K(sI - A + BK + LC)^{-1}LC(sI - A)^{-1}B \tag{8}$$

In all numerical examples that follow, the filter gains L are determined from Kalman filter theory with measurement noise intensity equal to the identity matrix and plant noise intensity equal to BB^T.

Table 1 Typical section properties

$K_\alpha = 11{,}963$ lb/ft	$K_h = 2991$ psf
$m = 1.196$ slug/ft	$I_\alpha = 1.196$ slug-ft
$S_\alpha = 0.239$ slug	$a = -0.4$
$c_L = -0.6$	$c_T = 0.6$
$\rho = 0.00238$ slug/ft^3	$b = 2$ ft
$\tau = 200$ rad/s	

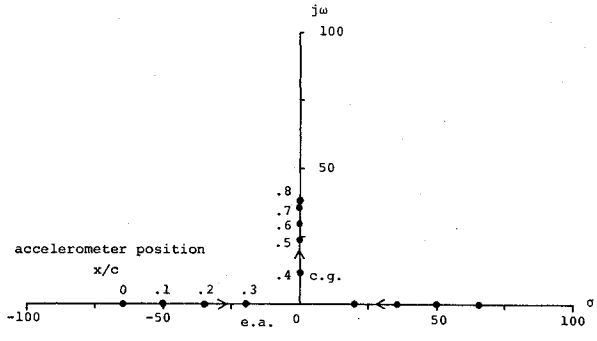

Fig. 3 Root locus of zeros for various chordwise accelerometer placements for trailing-edge control only.

Numerical Examples

The numerical results that follow are for the typical section properties (taken from Ref. 15) shown in Table 1. The leading- and trailing-edge control surfaces span 20% of the 4-ft chord at sea level.

The design condition for the flutter control laws will all be at a velocity of 125% of the flutter velocity.

Case 1

In this section, the numerical results for a control system based on a surface with a single trailing-edge control and single accelerometer are presented. In this single-input/single-output case, the characteristic equation for the open-loop flutter poles is easily determined as

$$\left[mI_\alpha - S_\alpha^2\right]p^4 + \left[m(K_\alpha - M_\alpha) - S_\alpha L_\alpha + I_\alpha K_h\right]p^2 + \left[K_h(K_\alpha - M_\alpha)\right] = 0 \tag{9}$$

The equation for the zeros is

$$\left[\ell_1 b(M_{\beta_T} m + S_\alpha L_{\beta_T}) - (M_{\beta_T} S_\alpha + L_{\beta_T} I_\alpha)\right]z^4 + \left[\ell_1 b M_{\beta_T} K_h - M_{\beta_T} L_\alpha - L_{\beta_T}(K_\alpha - M_\alpha)\right]z^2 = 0 \tag{10}$$

The open-loop root locus of Eq. (9) for varying velocity is shown in Fig. 2a and the closed-loop full state feedback in Fig. 2b. The flutter speed is at $U_F = 600$ ft/s. Notice that the right half-plane pole is flipped about the imaginary axis at the design velocity. The root locus of Eq. (10) for various chordwise accelerometer placements and $U = 1.25U_F = 750$ ft/s is shown in Fig. 3. From Fig. 3 we see that, in this case, as the accelerometer is moved from the leading edge rearward, the zeros move from the real axis to the imaginary axis. Two additional zeros at the origin are not shown in Fig. 3. Clearly, positions near the leading edge result in right half-plane zeros, and we might expect poor robustness recovery as a consequence in our observer design. The locations near the control surface hingeline have no right half-plane zeros, and we would expect good robustness recovery. Note that, in this example, the elastic axis is not a good candidate for sensor location because of the right half-plane zero.

In this single-input/single-output case, there is a single output transfer function, since the full state transfer function

$$G_R(s) = K(sI - A)^{-1}B$$

and the accelerometer feedback transfer function

$$G_0(s) = K(sI - A + BK + LC)^{-1} LC(sI - A)^{-1} B$$

are scalars. The stability robustness can be examined in classical terms from the Bode plots of these functions. Figure 4 presents the gain and phase plots of the full state and LTR designs for the leading edge, elastic axis, and control surface hinge accelerometer positions. It is clear that the positions yielding right half-plane zeros do not achieve anywhere near the degree of robustness recovery that the minimum phase hinge position does. There is a significant degradation in rms response as well as that shown in Table 2, which presents the closed-loop rms α, h, and β_T responses due to the white gust noise described earlier.

Case 2

In this section, the numerical results for a control system based on a surface with a single leading-edge control and a single accelerometer are presented. The characteristic pole equation is the same as Eq. (9), and the zeros equation is now

$$\left[\ell_2 b(M_{\beta_L} m + S_\alpha L_{\beta_L}) - (M_{\beta_L} S_\alpha + L_{\beta_L} I_\alpha)\right] z^4 + \left[\ell_2 b M_{\beta_L} K_h - M_{\beta_L} L_\alpha - L_{\beta_L}(K_\alpha - M_\alpha)\right] z^2 = 0 \qquad (11)$$

The root locus of Eq. (11) for various chordwise accelerometer placements is the complement of that in Fig. 3. Once again, minimum phase systems result when the accelerometers are near the control surface hinge. Figure 5 is the Bode plots of the full state and LTR designs for the control surface hinge, elastic axis, and trailing-edge accelerometer positions. Again it is clear that the trailing-edge accelerometer placement, which is the only nonminimum phase system, does not recover the loop transfer function very well, and should be avoided. Table 3 contains the rms gust response for these designs, and it is once again evident that the nonminimum phase system rms is worse than the minimum phase systems.

Case 3

In this section, the numerical results for a control system based on a surface with both leading- and trailing-edge controls, and two accelerometers are presented. The transmission zeros are independent of the accelerometer locations. All placements yield four zeros at the origin. The minimum singular value of the return difference matrix for this multi-input/multi-output system is depicted in Fig. 6 for three accelerometer combinations: 1) one at each control surface hinge, 2) one at the front hinge combined with one at the elastic axis, 3) one at the rear hinge combined with one at the elastic axis. The corresponding rms gust responses are tabulated in Table 4.

Since there are no right half-plane zeros arising, there is good robustness recovery for all designs shown in Fig. 6. The multi-input/multi-output system is, as one might expect, slightly less robust than the properly designed single-input/single-output systems. From Fig. 6 and Table 4, we see that no particular accelerometer placements are superior when both controls are present. In the work of Ref. 11, the author has found that when one examines various actuator failure modes, however, the hinge locations perform somewhat better.

Table 2 rms gust responses at the design velocity for trailing-edge control only

	Accelerometer position		
rms	Leading edge	Elastic axis	Control surface hinge
α	17.7	9.9	1.4
h	5.6	3.1	2.9
β_T	30.5	16.9	2.2

Table 3 rms gust responses at the design velocity for leading-edge control only

	Accelerometer position		
rms	Control surface hinge	Elastic axis	Trailing edge
α	0.095	0.065	0.35
h	0.46	0.42	2.3
β_L	0.61	0.43	1.6

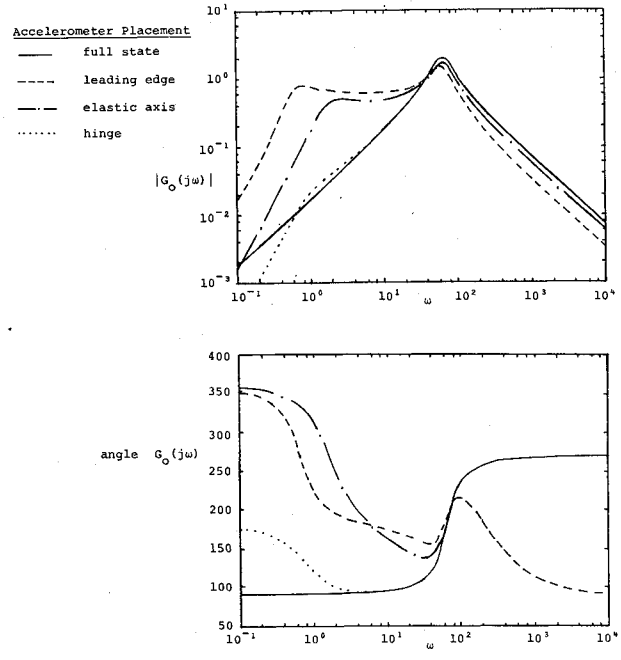

Fig. 4 Magnitude and phase of $G_0(j\omega)$ for trailing-edge control only.

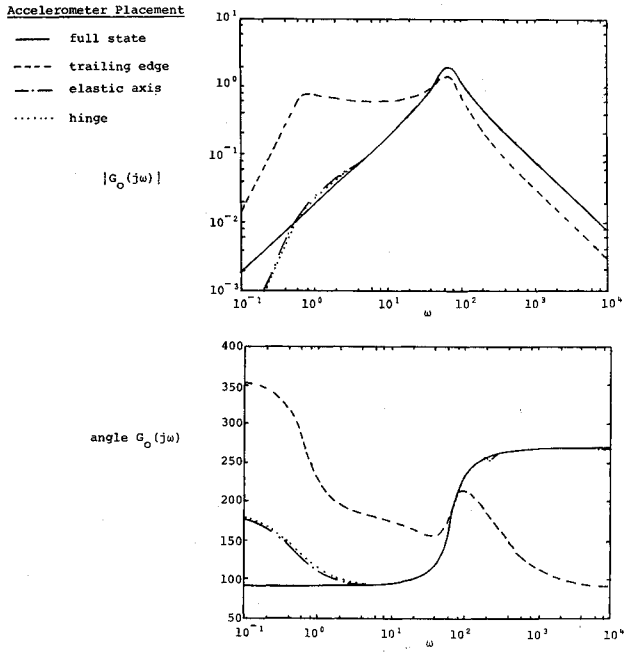

Fig. 5 Magnitude and phase of $G_0(j\omega)$ for leading-edge control only.

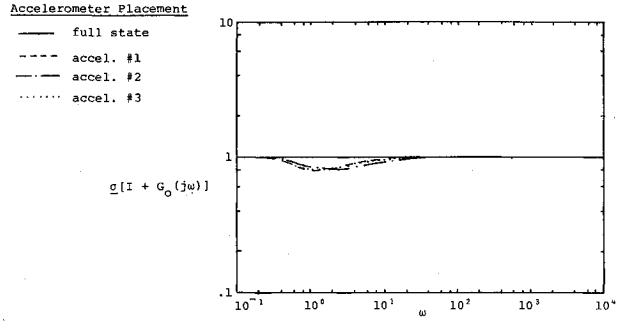

Fig. 6 Minimum singular value of return difference matrix for both leading- and trailing-edge controls.

Table 4 rms gust responses at the design velocity for both leading- and trailing-edge control

	Accelerometer position		
rms	Accelerometer position 1	Accelerometer position 2	Accelerometer position 3
α	1.5	2.2	1.5
h	2.7	2.2	2.2
β_T	3.4	4.6	3.2
β_L	2.3	2.1	1.9

Node Location

Let us determine the accelerometer location where transmission zeros switch from a complex conjugate pair to two reflexive real roots. This is certainly a critical location concerning robustness recovery. For the trailing-edge control location only, this can be found by solving for the ℓ_1 at which all four roots of Eq. (10) are zero. This is when the z^2 coefficient of Eq. (10) is zero, or

$$\ell_1 = \frac{M_{\beta_T} L_\alpha + L_{\beta_T}(K_\alpha - M_\alpha)}{b M_{\beta_T} K_h}$$

For the leading-edge case only, we can determine the node by solving for ℓ_2, where the coefficient of the z^4 term in Eq. (11) goes to zero.

$$\ell_2 = \frac{M_{\beta_L} S_\alpha + L_{\beta_L} I_\alpha}{b(M_{\beta_L} m + S_\alpha L_{\beta_L})}$$

In the present example, at the design velocity of 750 ft/s, the nodes are

$$\ell_1 = 0.16, \qquad \ell_2 = 0.27$$

Certainly, one wishes to remain as far from these nodes as possible to preclude any switching of the zeros from minimum phase to nonminimum phase due to model uncertainties. Thus, for a minimum phase system that is as insensitive to accelerometer placement as possible, we must place the accelerometer at the control surface hinge in each case. Hence, as shown here, the adage "place your sensors at your control inputs" certainly is applicable in flutter control by accelerometer feedback.

Since the magnitude of the measurements is small (for low-frequency inputs at the ℓ_1 node, and high-frequency inputs at the ℓ_2 node) at these points, one might choose to think of these points as inertial (or "nodal") points that move very little. Note that these nodes happen to bracket the c.g. ($\ell = 0.2$) location. This certainly matches physically with the high-frequency case where the mass center would tend to be immovable. The author has found this to be the case for other typical sections similar to the case examined, which implies that the c.g. could be used as a good indication of the nodal points in actual sections. The physical explanation for the phase shift across the nodal point can be readily interpreted in the following manner. Knowing that the nodes of the section tend to stay in place, the following can be surmised for the trailing-edge controller. When the control surface makes a positive motion, it will force the nose of the airfoil down and cause a negative (i.e., 180 deg out of phase from the input) vertical acceleration at points forward of the node. The accelerometers aft of the node will see the converse, and hence have the same phase as the input. A similar argument can be made for the leading-edge controller. Regardless of where the actual nodal points are, one would want to be on the minimum phase side and as far from it as possible, in fact at the two hinge locations.

Conclusions

The following conclusions are based upon the two-dimensional typical section model, and are, therefore, only qualitative in nature. Actual node locations for three-dimensional wings should be determined with much more complex models than were presented here. However, the present analysis demonstrates that robustness recovery attempts by loop-transfer-recovery methods in flutter suppression systems utilizing accelerometers as sensors will likely fail if the accelerometer placements are such that they result in right half-plane transmission zeros. Proper placement to assure minimum phase systems are:

1) For systems with one accelerometer and one control surface, either leading- or trailing-edge, the accelerometer should be placed near the control surface hingeline for maximum stability robustness.

2) For systems with both a leading- and trailing-edge control surface and two accelerometers, robustness is insensitive to accelerometer placement.

3) The section c.g. is a good indication of the location of the critical chordwise accelerometer position, where the system switches from minimum to nonminimum phase.

Acknowledgment

This research was partially supported by Grant NAG-1-217 from NASA Langley Research Center.

References

[1]Garrick, I.E., "Aeroelasticity—Frontiers and Beyond," AIAA Paper 76-219, 1976.

[2]"B-52 CCV Control System Synthesis," AFFDL-TR-74-92, Vol. II, Jan. 1975.

[3]Roger, K.L., Hodges, G.E., and Felt, L., "Active Flutter Suppression—A Flight Test Demonstration," *Journal of Aircraft*, Vol. 12, June 1975, pp. 551–556.

[4]"Supersonic Transport Flutter SAS Conceptual Study Results," The Boeing Co., Wichita Division, Rept. D3-7600-9, 1969.

[5]Gangsaas, D. and Ly, U., "Application of Modified Linear Quadratic Gaussian Design to Active Control of Transport Aircraft," AIAA Paper 79-1746, Aug. 1979.

[6]Murrow, H.N. and Eckstrom, C.V., "Drones for Aerodynamic and Structural Testing (DAST)—A Status Report," *Journal of Aircraft*, Vol. 16, Aug. 1979, pp. 521–526.

[7]Abel, P. and Murrow, H., "Two Synthesis Techniques Applied to Flutter Suppression on a Flight Research Wing," *Journal of Guidance, Control and Dynamics*, Vol. 1, Sept.-Oct. 1978, pp. 340–346.

[8]Mahesh, J., Stone, C., Garrard, W., and Dunn, H., "Control Law Synthesis for Flutter Suppression Using Linear Quadratic Gaussian Theory," *Journal of Guidance, Control and Dynamics*, Vol. 4, July–Aug. 1981, pp. 415–422.

[9]Garrard, W.L. and Liebst, B.S., "Active Flutter Suppression Using Eigenspace and Linear Quadratic Design Techniques," *Journal of Guidance, Control and Dynamics*, Vol. 8, May–June 1985, pp. 304–311.

[10]Liebst, B.S., Garrard, W.L., and Adams, W.M., "Design of an Active Flutter Suppression System," *Journal of Guidance, Control and Dynamics*, Vol. 9, Feb. 1986, pp. 64–71.

[11]Liebst, B.S., Garrard, W.L., and Farm, J.A., "Design of a Multivariable Flutter Control/Gust Load Alleviation System," AIAA Paper 86-2247, *Proceedings AIAA Guidance and Control Conference*, Williamsburg, VA, Aug. 1986, pp. 835–847.

[12]Cannon, R.H. and Rosenthal, D.E., "Experiments in Control of Flexible Structures with Noncollocated Sensors and Actuators," *Journal of Guidance, Control and Dynamics*, Vol. 7, Sept.–Oct. 1984, pp. 546–553.

[13]Bryson, A.E. and Wie, B., "Modeling and Control of Flexible Space Structures," *Proceedings of the Third Symposium on Dynamics and Control of Large Flexible Spacecraft*, Blacksburg, VA, June 1981, pp. 153–174.

[14]Dowell, E.H. and Horikawa, H., "An Elementary Explanation of Flutter Mechanism with Active Feedback Controls," *Journal of Aircraft*, Vol. 16, April 1979, pp. 225–232.

[15]Edwards, J.W., "Unsteady Aerodynamic Modeling and Active Aeroelastic Control," Stanford University Center for System Research, Rept. SUDAAR 504, 1977.

[16]Doyle, J.C. and Stein, G., "Robustness with Observers," *IEEE Transactions on Automatic Control*, Vol. AC-24, Aug. 1979, pp. 607–610.

[17]Theodorsen, T., "General Theory of Aerodynamic Instability and the Mechanism of Flutter," NACA Rept. 496, 1935.

[18]Safanov, M., Laub, A., and Hartmann, G., "Feedback Properties of Multivariable Systems: The Role and Use of the Return Difference Matrix," *IEEE Transactions on Automatic Control*, Vol. AC-26, Feb. 1981, pp. 47–65.